



## Research Article

<https://doi.org/10.1631/jzus.B2100187>



# Transition of autophagy and apoptosis in fibroblasts depends on dominant expression of HIF-1 $\alpha$ or p53

Min LI<sup>1</sup>, Yidan SU<sup>2</sup>, Xiaoyuan GAO<sup>1</sup>, Jiarong YU<sup>1</sup>, Zhiyong WANG<sup>1</sup>✉, Xiqiao WANG<sup>1</sup>✉

<sup>1</sup>Department of Burn, Ruijin Hospital, Shanghai Jiao Tong University School of Medicine, Shanghai 200025, China

<sup>2</sup>Department of Plastic Surgery, Shanghai Changzheng Hospital, Shanghai 200003, China

**Abstract:** It has been revealed that hypoxia is dynamic in hypertrophic scars; therefore, we considered that it may have different effects on hypoxia-inducible factor-1 $\alpha$  (HIF-1 $\alpha$ ) and p53 expression. Herein, we aimed to confirm the presence of a teeterboard-like conversion between HIF-1 $\alpha$  and p53, which is correlated with scar formation and regression. Thus, we obtained samples of normal skin and hypertrophic scars to identify the differences in HIF-1 $\alpha$  and autophagy using immunohistochemistry and transmission electron microscopy. In addition, we used moderate hypoxia in vitro to simulate the proliferative scar, and silenced *HIF-1 $\alpha$*  or *p53* gene expression or triggered overexpression to investigate the changes of HIF-1 $\alpha$  and p53 expression, autophagy, apoptosis, and cell proliferation under this condition. HIF-1 $\alpha$ , p53, and autophagy-related proteins were assayed using western blotting and immunofluorescence, whereas apoptosis was detected using flow cytometry analysis, and cell proliferation was detected using cell counting kit-8 (CCK-8) and 5-bromo-2'-deoxyuridine (BrdU) staining. Furthermore, immunoprecipitation was performed to verify the binding of HIF-1 $\alpha$  and p53 to transcription cofactor p300. Our results demonstrated that, in scar tissue, HIF-1 $\alpha$  expression increased in parallel with autophagosome formation. Under hypoxia, HIF-1 $\alpha$  expression and autophagy were upregulated, whereas p53 expression and apoptosis were downregulated in vitro. HIF-1 $\alpha$  knockdown downregulated autophagy, proliferation, and p300-bound HIF-1 $\alpha$ , and upregulated p53 expression, apoptosis, and p300-bound p53. Meanwhile, p53 knockdown induced the opposite effects and enhanced HIF-1 $\alpha$ , whereas p53 overexpression resulted in the same effects and reduced HIF-1 $\alpha$ . Our results suggest a teeterboard-like conversion between HIF-1 $\alpha$  and p53, which is linked with scar hyperplasia and regression.

**Key words:** Hypertrophic scar; Hypoxia-inducible factor-1 $\alpha$  (HIF-1 $\alpha$ ); p53; Autophagy; Apoptosis

## 1 Introduction

Hypertrophic scars (HSs), the most common complication of abnormal healing after burns and thermal injuries, are characterized by excessive fibroblast proliferation and collagen production that lead to severe cosmetic and functional impairment (Gauglitz et al., 2011; van den Broek et al., 2014; Finnerty et al., 2016; Chen et al., 2021).

During scar progression, extensive microvessels are formed at the hyperplasia stage, most of which later become partially or totally occluded, resulting in

dynamic hypoxia in scar tissue. This was reported as moderate during the proliferative stage, but severe during the regression stage (Zheng et al., 2014; Dong et al., 2016; Qing et al., 2016). Although the fibroblast characteristics are dynamic (Qing et al., 2016), the mechanism by which dynamic hypoxia regulates fibroblasts and scar formation is poorly understood.

In recent years, cell survival and death were considered to be correlated with autophagy and apoptosis under a hypoxic environment. Autophagy is a conserved catabolic process of cells, during which double-membrane autophagosomes deliver cytoplasmic contents to lysosomes for degradation. The structures for degradation include misfolded proteins, damaged and dysfunctional organelles, and lipids, and the degraded products are utilized by cells for survival. The inhibition of cell autophagy induces apoptosis; therefore, autophagy is essential for maintaining homeostasis, and to prevent the development of pathological

✉ Xiqiao WANG, wxqiao2002@hotmail.com

Zhiyong WANG, wzy10830@tjh.com.cn

Zhiyong WANG, <https://orcid.org/0000-0001-9265-3719>

Xiqiao WANG, <https://orcid.org/0000-0002-2139-9853>

Received Feb. 26, 2021; Revision accepted Aug. 10, 2021;

Crosschecked Feb. 28, 2022

© Zhejiang University Press 2022

states such as neurodegenerative disease, cancer, and ageing (Levine and Kroemer, 2019).

Hypoxia likely regulates autophagy through the hypoxia-inducible factor-1 (HIF-1) (Xia et al., 2015; Wang et al., 2018; Deng et al., 2020). It is a hypoxia-responsive heterodimeric transcription factor that binds to hypoxia response elements and triggers the expression of genes controlling various cellular functions (Ratcliffe et al., 1998; Ivan et al., 2001; Jaakkola et al., 2001), including metabolism, survival, proliferation, and autophagy (Harris, 2002). The expression of HIF-1 $\alpha$  is upregulated in HS fibroblasts (Wu et al., 2018). During HS regression, HIF-1 $\alpha$  expression is reduced along with increased p53 expression and cell apoptosis (Lynam et al., 2015; Dong et al., 2016).

Under normal conditions, cell apoptosis is controlled by p53 expression (Nuñez-Hernandez et al., 2018). Low levels of p53 are expressed under normoxia and p53 is stably expressed during severe hypoxia (Shieh et al., 1997; Zhang and Xiong, 2001). The overexpression of p53 inhibits HSs by downregulating fibroblast proliferation and collagen deposition (Liang et al., 2021).

The above evidence suggests that, during scar formation and regression, dynamic hypoxia has different effects on the expression of HIF-1 $\alpha$  and p53. Therefore, in this study, we aimed to investigate the presence of a teeterboard-like conversion between HIF-1 $\alpha$  and p53, which is likely correlated with fibroblast autophagy and apoptosis, ultimately causing scar formation and regression. In addition, we analyzed the possible internal factors that link HIF-1 $\alpha$  and p53 and regulate their expression. We obtained samples of normal skin and HSs to determine differences in HIF-1 $\alpha$  and autophagy. In addition, we used moderate hypoxia *in vitro* to simulate proliferative scars and silenced *HIF-1 $\alpha$*  or *p53* expression, or triggered overexpression to investigate the changes of HIF-1 $\alpha$  and p53 expression, autophagy, apoptosis, and cell proliferation.

## 2 Materials and methods

### 2.1 Clinical samples

Sections of HSs in the proliferative stage and normal skin were obtained from the operating room of the Burn Department of Ruijin Hospital affiliated to Shanghai Jiao Tong University School of Medicine,

Shanghai, China. Six patients (three males and three females) aged 20 to 56 years with burn-related HSs (6–12 months after wound healing) on their upper limbs were recruited for this study, and keloids were excluded. The control tissues were the discarded normal skin trimmed off during the skin transplantation operation.

### 2.2 Transmission electron microscopy (TEM)

Samples of HSs and normal skin were cut into about 1-mm<sup>3</sup> cubes. The specimens were fixed with 2.5% (volume fraction) glutaraldehyde followed by 1% (volume fraction) OsO<sub>4</sub>, placed on ice, and stored at 4 °C. Next, the samples underwent serial dehydration, soaking, embedding in epoxy resin, and sectioning into ultrathin 60-nm sections. These were stained with a solution of uranyl acetate and lead citrate, and a transmission electron microscope (Hitachi 500, Hitachi, Ltd., Tokyo, Japan) was used at a voltage of 75 kV to observe the microstructural changes in fibroblasts within the tissues. The area of autophagic vesicles was calculated using ImageJ software (Schneider et al., 2012), and the ratios of total area of autophagic vesicles and cytoplasmic area (cell area minus nuclear area) were then determined. Three samples were included in each group, and three fields were taken for each sample.

### 2.3 Immunohistochemistry (IHC)

The normal skin and HS samples were embedded in paraffin, sectioned, dewaxed, subjected to antigen retrieval, ruptured, sealed with 3% (volume fraction) bovine serum albumin (BSA) for 30 min, and placed in a humid box with HIF-1 $\alpha$  primary antibody (1:50 (volume ratio), NB100-105, Novus Biologicals Inc., Littleton, CO, USA) at room temperature for overnight incubation. Next, they were incubated with the secondary antibody for 50 min and developed by 3,3'-diaminobenzidine tetrahydrochloride (DAB, brown positive staining). The nuclei were counterstained by haematoxylin and finally dehydrated and mounted. Subsequently, they were observed under a microscope (Axiovert 200, Zeiss, Germany) with 200 $\times$  magnification and imaged. The percentage of positive cells was calculated using ImageJ's Trainable Weka Segmentation plug-in. The sample size of each group was five and five fields were randomly selected for each sample.

## 2.4 Cell culture

Human dermal fibroblasts (HDFs; Cat. No. 2320; Shanghai Zhong Qiao Xin Zhou Biotechnology Co., Ltd., Shanghai, China) were incubated in high-glucose Dulbecco's modified Eagle's medium (DMEM) supplemented with 10% (volume fraction) fetal bovine serum (FBS) and 1% (volume fraction) antibiotics at 37 °C under a humidified 5% CO<sub>2</sub> atmosphere. The HDFs were treated in DMEM under 5% O<sub>2</sub>/5% CO<sub>2</sub> at 37 °C to simulate moderate hypoxia (Dong et al., 2016), and then assayed after 0, 6, 12, 24, and 48 h.

## 2.5 Lentiviral vector construction and transfection

Lentiviral short hairpin RNA HIF-1 $\alpha$  (sh-HIF-1 $\alpha$ ) and sh-p53, as well as p53 overexpression (p53<sup>OE</sup>) vectors, were constructed and packaged (Jikai Gene, Shanghai, China), and then transfected into about 30% confluent HDFs for 16 h. The medium was replaced, and the transfection efficiency was visualized by microscopy after 72 h as green fluorescence protein. The transfected HDFs were then cultured and screened in DMEM containing puromycin. Levels of HIF-1 $\alpha$  and p53 were detected using quantitative real-time polymerase chain reaction (qRT-PCR) and western blotting. The changes in autophagy, apoptosis, and proliferation of transfected HDFs were assayed after treatment under moderate hypoxia for 48 h.

## 2.6 Cell proliferation assay

The cell proliferation assay procedure is described below. HDFs (2 $\times$ 10<sup>3</sup> cells/well) were inoculated into the 96-well plates. The original medium was replaced after 24 h with the same medium containing 5% FBS, and the cells were incubated at 37 °C under a 5% O<sub>2</sub>/5% CO<sub>2</sub> atmosphere for 0, 24, and 48 h, followed by the cell counting kit-8 (CCK-8) reagent for 2 h at 37 °C. Absorbance at 450 nm was measured using an Epoch Ultra Microplate Spectrophotometer (Agilent Technologies Inc., Santa Clara, CA, USA). Transfected HDFs (4 $\times$ 10<sup>3</sup> cells/well) were inoculated into Millicell<sup>®</sup> EZ slides (PEZGS0816, Millipore Sigma Co., Ltd., Burlington, MA, USA). After 24 h, the original medium was replaced with medium containing 5% FBS and 5-bromo-2'-deoxyuridine (BrdU) at a final concentration of 1 mg/mL. Subsequently, the cells were incubated at 37 °C under a 5% O<sub>2</sub>/5% CO<sub>2</sub> atmosphere for 48 h, then fixed, denatured, and neutralized, and the nonspecific protein binding was blocked. Next, the

cells were incubated with an anti-BrdU primary antibody (1:250 (volume ratio), ab6326, Abcam, Cambridge, UK) overnight at 4 °C, washed three times with phosphate-buffered saline (PBS), and incubated with a secondary antibody (1:1000, A21434, Thermo Fisher Scientific Inc., Waltham, MA, USA) for 1 h at room temperature in the dark and washed three times with PBS. Thereafter, nuclei were stained with diisopropanolamine (DIPA)-containing anti-fluorescence quencher (36308ES20, Yeasen, Shanghai, China), and the cells were visualized using a fluorescence microscope (200 $\times$  magnification; Axiovert 200, Zeiss, Germany). The ratio of BrdU-positive cells was counted. The sample size of each group was three, whereas eight fields were selected for each sample.

## 2.7 Western blotting

The HDF samples treated with different periods of hypoxia, and sh-HIF-1 $\alpha$ , sh-p53, p53<sup>OE</sup>, and the corresponding negative control HDFs treated with hypoxia for 48 h were used for western blot ( $n=3$  per group). The levels of autophagy-related proteins (light chain 3 (LC3), Beclin-1, p62), HIF-1 $\alpha$ , p53, type III collagen, p300, and  $\beta$ -actin in HDFs were detected by western blotting as follows. Briefly, total protein (25  $\mu$ g) from each sample was separated on 4%–12% Precast Gel (180-8008H, Tanon Science and Technology Co., Shanghai, China) and transferred onto polyvinylidene difluoride (PVDF) membranes. After blocking nonspecific protein binding on the PVDF membranes in 5% (0.05 g/mL) skimmed milk for 1 h, the membranes were incubated with primary antibodies against LC3 (1:1000, ab51520, Abcam), Beclin-1 (1:1000, ab62557, Abcam), p62 (1:1000, ab56416, Abcam), HIF-1 $\alpha$  (1:500, NB100-105, Novus), p53 (1:1000, 2527S, Cell Signaling Technology Inc., Boston, MA, USA), collagen III (1:1000, 22734-1-AP, Proteintech, Wuhan, China), and  $\beta$ -actin (1:5000, 66009-1-Ig, Proteintech) at 4 °C overnight, followed by secondary antibodies for 1 h at room temperature. The signals were visualized using ECL substrate (Millipore Sigma) and the model 4600 enhanced chemiluminescence system (Tanon). The protein band intensity was determined using ImageJ software through the freehand tool, the protein levels were standardized against  $\beta$ -actin, and the data were normalized to the control group.

## 2.8 qRT-PCR

We extracted RNA from HDFs using TRIzol reagent (Invitrogen, USA) as instructed by the manufacturer. Complementary DNA (cDNA) was synthesized using ReverTra Ace™ qPCR RT Kits (FSQ-101, Toyobo Co., Ltd., Osaka, Japan), and qRT-PCR amplification was performed using SYBR Green Realtime PCR Master Mix (QPK-201, Toyobo) in the Applied Biosystems™ 7500 Fast Real-time PCR System (Thermo Fisher). The forward and reverse synthesized PCR primers (Sangon Biotech Co., Ltd., Shanghai, China) were respectively as follows (5'→3'): *p53*, GAGGTTGGCTCTGACTGTACC and TCCGTCCCAGTAGATTACCAC; *HIF-1α*, GAA CGTCGAAAAGAAAAGTCTCG and CCTTATCA AGATGCGAACTCACA; *β-actin*, CTGTCCCTGTA TGCCTCTG and ACTCACCATGCTGTGCTGGTTC. The level of messenger RNA (mRNA) expression was standardized based on *β-actin* expression, and target gene expression was determined relative to the expression in the control using the  $2^{-\Delta\Delta C_t}$  method.

## 2.9 Flow cytometry of cell apoptosis

The apoptosis rate was determined by flow cytometry using the Annexin-V-allophycocyanin (APC) apoptosis detection kit (BD Biosciences, San Jose, CA, USA). HDFs were seeded in six-well plates, which were left to stand overnight, the medium was replaced with one containing 5% FBS, and cells were cultured for 0, 6, 12, 24, and 48 h in 5% O<sub>2</sub>. Transfected HDFs were cultured under moderate hypoxia for 48 h, digested with 0.25% (2.5 g/L) trypsin, and pelleted using centrifugation at 1500 r/min for 5 min. The cells were then incubated with Annexin-V-APC in the dark for 15 min, and 7-amino-actinomycin D (7-AAD) or propidium iodide (PI) was added to each sample before assessment using a CytoFlex S flow cytometer (Beckman Coulter Inc., Brea, CA, USA). The results were analyzed using FlowJo™ software (BD Biosciences).

## 2.10 Immunofluorescence staining and confocal microscopy

Transfected HDFs were inoculated into Millicell EZ slides (4×10<sup>3</sup> cells/well). The original medium was replaced with fresh medium containing 5% FBS, and the cells were incubated at 37 °C under a 5% O<sub>2</sub>/5% CO<sub>2</sub> atmosphere for 48 h. Next, the cells were fixed in

4% (volume fraction) paraformaldehyde for 20 min and permeabilized with 0.5% (volume fraction) Triton X-100 for 30 min, and nonspecific protein binding was blocked with 5% (volume fraction) BSA for 1 h at 4 °C. The cells were then incubated with LC3 primary antibody overnight at 4 °C, followed by secondary antibody at room temperature for 1 h, and nuclei were stained. The cells were visualized using a Zeiss 880 confocal microscope (Carl Zeiss Microscopy GmbH, Jena, Germany), and the number of endogenous LC3 puncta (diameter: 0.75–1.50 μm) per cell was counted using Adobe Photoshop software with the help of a ruler tool. The sample size of each group was five, and five fields were selected for each sample.

## 2.11 Immunoprecipitation and western blot analysis

Transfected HDFs were incubated under hypoxia for 48 h and washed twice with PBS, then radio immunoprecipitation assay (RIPA) buffer and phenylmethylsulfonyl fluoride (PMSF) were added for 5 min, and the cells were placed on ice for 10 min. The supernatant was collected by centrifugation at 4 °C and 14000g for 10 min, and then placed on ice. A volume of 25 μL suspension of protein A/G immunoprecipitation magnetic beads (Bimake, Houston, TX, USA) was mixed with 200 μL of binding buffer in 1.5-mL Eppendorf tubes. The immunoprecipitates were magnetically separated (Bimake) and then aspirated. The supernatant was discarded and the immunoprecipitates on beads were washed twice. Next, anti-p300 primary antibodies (4 μL) and antigen (400 μL) were added to the beads and gently dispersed using a pipette. The suspension was left to react overnight at 4 °C in an inversion mixer. Subsequently, the beads were magnetically separated from the antibody-antigen complexes. The supernatant was aspirated, 200 μL washing buffer was added to the tubes, and the suspension was gently pipetted to evenly disperse the magnetic bead-antibody-antigen complex for magnetic separation. Thereafter, the supernatant was aspirated and discarded, and then the complexes were washed twice and suspended in 200 μL of washing buffer, which was pipetted into new 1.5-ml EP tubes, followed by another magnetic separation and aspiration of the supernatant. The samples were then kept at 95 °C for 5 min in 50 μL of 1× sodium dodecyl sulfate-polyacrylamide gel electrophoresis (SDS-PAGE) loading buffer. The magnetic separation was repeated

and the supernatant was finally collected for western blotting.

## 2.12 Statistical analysis

All data were statistically analyzed using GraphPad Prism 9.0 (GraphPad Software Inc., San Diego, CA, USA). The data were expressed as mean±standard deviation (SD). The unpaired *t*-test was used for two independent groups ( $n=3$ ), and the Welch test was employed when the data did not follow normal distribution. The nested *t*-test was used for the statistical analysis of TEM autophagic vesicle area ( $n=3$ ), IHC HIF-1 $\alpha$  expression ( $n=3$ ), LC3 fluorescent staining ( $n=5$ ), and BrdU staining ( $n=3$ ). One-way analysis of variance (ANOVA) and Dunnett's multiple comparison test were performed for control and hourly comparisons ( $n=3$ ). Two-way ANOVA and Sidak multiple comparisons were used for CCK-8 analysis ( $n=12$ ).  $P<0.05$  was considered statistically significant.

## 3 Results

### 3.1 Upregulated HIF-1 $\alpha$ expression and autophagy in HS tissue at the proliferative stage

The autophagy levels were compared between HS and normal tissues using TEM. Compared with

normal skin, autophagosomes were significantly increased during the proliferative stage in the HS group ( $P=0.0002$ ; Figs. 1a–1c). HIF-1 $\alpha$  expression was compared in tissue samples using IHC, and it was also significantly higher in proliferating HSs ( $P=0.0002$ ; Figs. 1d–1f). These results demonstrated that both HIF-1 $\alpha$  and autophagy were upregulated in the proliferative stage of HSs.

### 3.2 Upregulated HIF-1 $\alpha$ expression, autophagy, and proliferation, and downregulated p53 expression and apoptosis in HDFs under moderate hypoxia

The HDFs were cultured under moderate hypoxia to simulate the environment of HSs in the proliferative stage. The western blotting results revealed the time-dependent upregulation and downregulation of HIF-1 $\alpha$  and p53 proteins, respectively (Figs. 2a–2c). The function of autophagy requires the participation of a variety of autophagy-related proteins, including LC3 and Beclin-1. The former is an essential part of the autophagosome membrane and an important autophagy marker (Morishita et al., 2017). The newly synthesized pro-LC3 is processed into cytoplasmic LC3-I, and then a small fragment of peptide is digested and converted into membrane LC3-II (Kabeya et al., 2000). As a mammalian homolog of yeast Atg6, Beclin-1 plays a crucial role in the initiation and formation of autophagosome-related complexes (He and

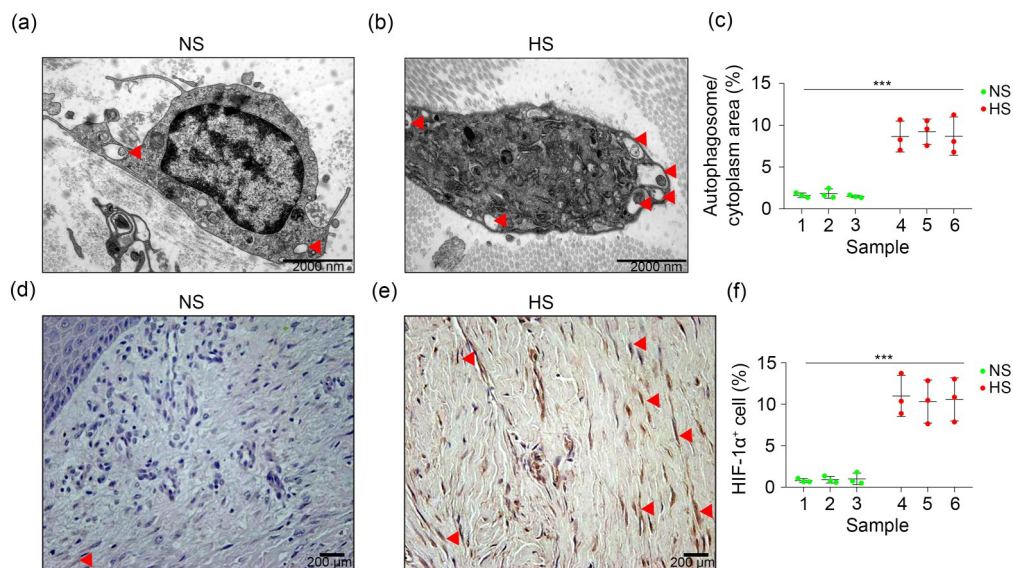


**Fig. 1** Autophagy levels and HIF-1 $\alpha$  expression were upregulated in HS tissue at the proliferative stage. (a–c) Autophagosome levels in NS and HS tissues determined by TEM, as indicated by the arrowheads ( $n=3$ ); (d–f) Expression of HIF-1 $\alpha$  in NS and HS tissues determined by IHC, as indicated by the arrowheads ( $n=3$ ). NS: normal skin; HS: hypertrophic scar; HIF-1 $\alpha$ : hypoxia inducible factor-1 $\alpha$ ; TEM: transmission electron microscopy; IHC: immunohistochemistry. \*\*\*  $P<0.001$ .

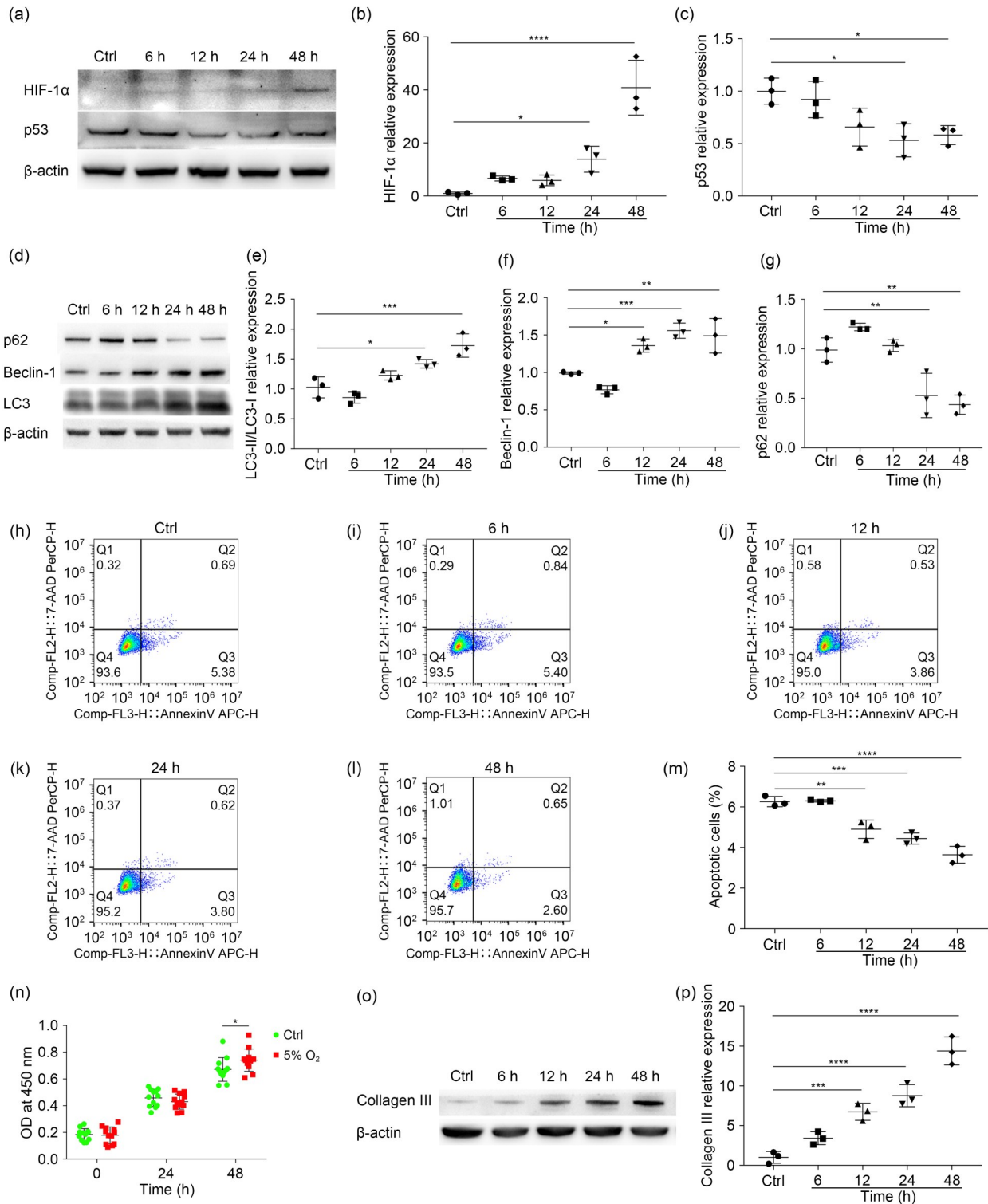


**Fig. 2** HIF-1α expression, autophagy, and proliferation are upregulated, while p53 expression and apoptosis are downregulated in HDFs under moderate hypoxia. (a–g) Western blots of HIF-1α, p53, LC3-II/LC3-I, Beclin-1, and p62 proteins ( $n=3$ ); (h–m) Apoptosis rates determined using flow cytometry ( $n=3$ ); (n) Cell proliferation under normal or moderate hypoxia determined using CCK-8 assay ( $n=12$ ); (o, p) Western blots of type III collagen ( $n=3$ ). Control cells were cultured without hypoxia. Cells were incubated under hypoxia for different periods. \*  $P<0.05$ , \*\*  $P<0.01$ , \*\*\*  $P<0.001$ , \*\*\*\*  $P<0.0001$ . HIF-1α: hypoxia inducible factor-1α; HDF: human dermal fibroblast; LC3: light chain 3; CCK-8: cell counting kit-8; Ctrl: control; OD: optical density.

Klionsky, 2009; Sun et al., 2018). The p62 protein is directly polyubiquitinated or monoubiquitinated with LC3 through its ubiquitin-related domain and is connected to the ubiquitinated substrate for degradation by autophagy lysosomes (Bjørkøy et al., 2005; Pankiv et al., 2007). The expression levels of LC3-II/LC3-I, Beclin-1, and p62 can reflect the level of autophagy. Autophagy was found to be gradually enhanced in HDFs under prolonged moderate hypoxia exposure. The protein expression of LC3-II/LC3-I and Beclin-1 increased, while that of p62 decreased (Figs. 2d–2g). In contrast to autophagy, apoptosis decreased in a time-dependent fashion (Figs. 2h–2m). We investigated whether moderate hypoxia impacts cell proliferation, and found that cell proliferation in the control and under moderate hypoxia after 24 h did not significantly differ. However, proliferation under moderate hypoxia was significantly increased after 48 h (Fig. 2n). In addition, the protein expression of type III collagen gradually increased in parallel with the duration of moderate hypoxia (Figs. 2o and 2p). Taken together, moderate hypoxia enhanced HIF-1 $\alpha$  expression, autophagy, and proliferation, and suppressed p53 expression and apoptosis in HDFs. The corresponding data are shown in Table S1.

### 3.3 Downregulated HIF-1 $\alpha$ expression, autophagy, and proliferation, and upregulated p53 expression and apoptosis in sh-HIF-1 $\alpha$ HDFs under moderate hypoxia

qRT-PCR was performed to quantify the mRNA expression of *HIF-1 $\alpha$* . The findings indicated that the mRNA (Fig. 3a) and protein (Figs. 3b and 3c) expression levels of HIF-1 $\alpha$  were significantly downregulated in sh-HIF-1 $\alpha$ -transfected (73007) HDFs. Thus, sh-HIF-1 $\alpha$ -transfected (73007) HDFs were used for subsequent experiments. After culture in 5% O<sub>2</sub> for 48 h, p53 expression was upregulated (Figs. 3o and 3q). Regarding autophagy, LC3-II/LC3-I and Beclin-1 were decreased, whereas p62 level was enhanced (Figs. 3d–3g). Immunofluorescence staining revealed significantly fewer LC3 puncta in sh-HIF-1 $\alpha$ -transfected cells as compared with control cells ( $P < 0.0001$ ; Figs. 3h and 3i). These findings indicated autophagy in both cell lines, but it was suppressed in sh-HIF-1 $\alpha$  HDFs. The flow cytometry findings revealed enhanced apoptosis in sh-HIF-1 $\alpha$  HDFs (Figs. 3j–3l). The ratios of BrdU-positive cells were lower after HIF-1 $\alpha$

knockdown, indicating reduced cell proliferation ( $P = 0.0023$ ; Figs. 3m and 3n). In addition, the protein expression of type III collagen was also decreased after HIF-1 $\alpha$  knockdown (Figs. 3o and 3p). These results indicated that HIF-1 $\alpha$ , collagen III, autophagy, and proliferation were downregulated, while p53 levels and apoptosis were enhanced under moderate hypoxia in sh-HIF-1 $\alpha$ . The relevant data are shown in Table S2.

### 3.4 Upregulated HIF-1 $\alpha$ expression, autophagy, and proliferation, and suppressed p53 expression and apoptosis in sh-p53 HDFs under moderate hypoxia

The mRNA expression of *p53* was the most significantly downregulated in sh-p53 (92365) HDFs (Fig. 4a), which was also confirmed at the protein level using western blotting (Figs. 4b and 4c). Thus, sh-p53 (92365) HDFs were included in subsequent experiments. After culture in 5% O<sub>2</sub>+5% FBS for 48 h, more HIF-1 $\alpha$  protein was expressed in p53 knockdown cells as compared with the controls (Figs. 4o and 4q). The protein expression of LC3-II/LC3-I and Beclin-1 also increased, whereas that of p62 was lower (Figs. 4d–4g). Immunofluorescence staining revealed LC3 puncta in both the control and knockdown cells, but their numbers were higher in the latter ( $P < 0.0001$ ; Figs. 4h and 4i). This indicated that autophagy was upregulated in sh-p53 HDFs. The flow cytometry findings revealed a lower rate of apoptosis in sh-p53 HDFs (Figs. 4j–4l). Furthermore, the ratios of BrdU-positive cells increased after p53 knockdown, indicating enhanced cell proliferation ( $P = 0.0004$ ; Figs. 4m and 4n). Type III collagen expression also increased after p53 knockdown (Figs. 4o and 4p). Taken together, these results indicated that moderate hypoxia upregulates HIF-1 $\alpha$ , autophagy, and proliferation, while it suppresses p53 and apoptosis in sh-p53 cells. The associated data are shown in Table S2.

### 3.5 Suppressed autophagy, proliferation, and HIF-1 $\alpha$ expression, and upregulated p53 expression and apoptosis in p53<sup>OE</sup> HDFs under moderate hypoxia

The mRNA (Fig. 5a) and protein (Figs. 5b and 5c) expression of p53 increased in p53<sup>OE</sup> (60933) HDFs. After 48 h of culture in 5% FBS under a 5% O<sub>2</sub> atmosphere, HIF-1 $\alpha$  protein expression was reduced in p53<sup>OE</sup> (60933) HDFs (Figs. 5o and 5q). Regarding autophagy, LC3-II/LC3-I and Beclin-1 were also downregulated, whereas the level of p62 protein increased

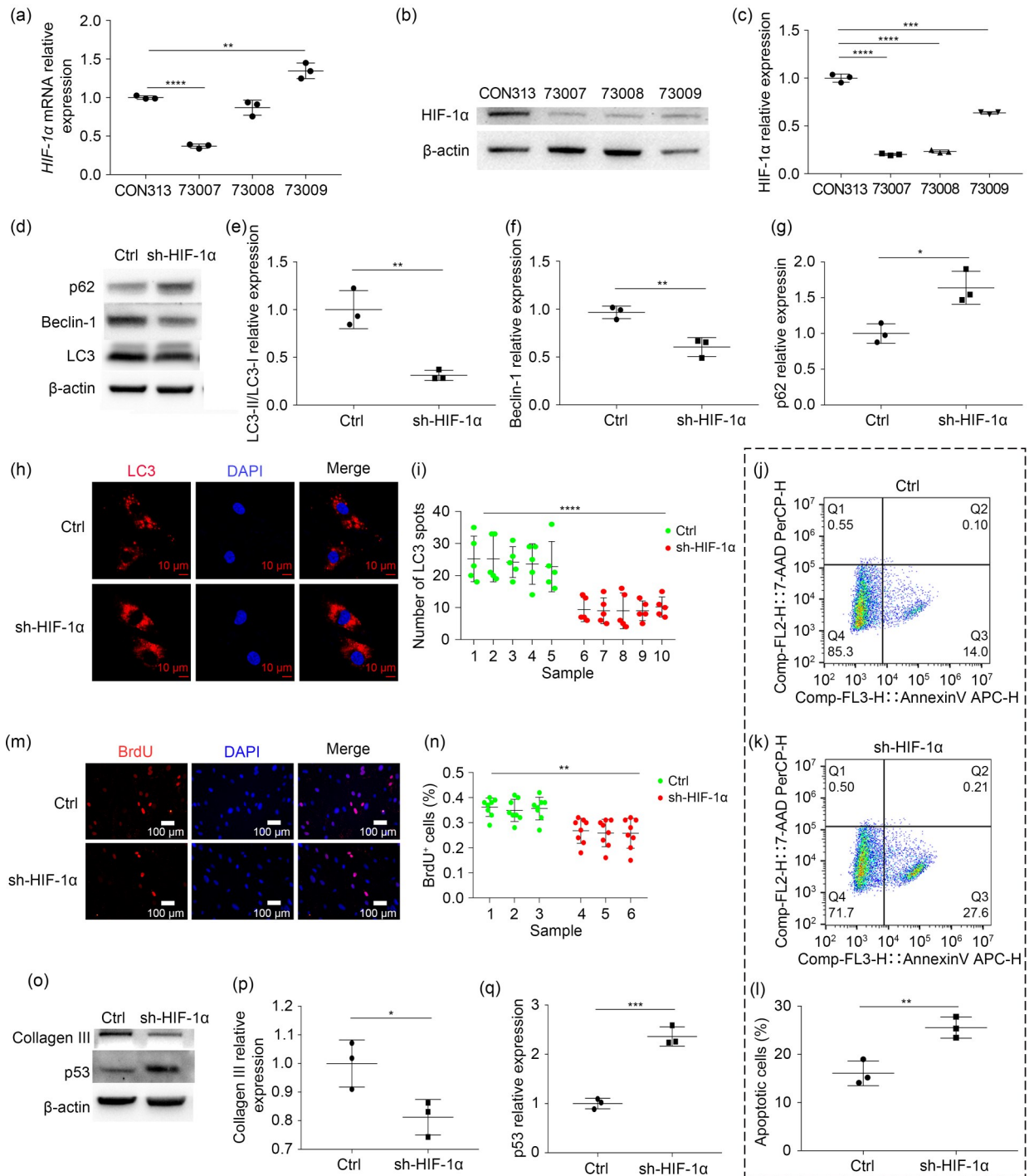


**Fig. 3** Moderate hypoxia suppresses *HIF-1 $\alpha$*  expression, autophagy, and proliferation, but enhances p53 expression and apoptosis in sh-*HIF-1 $\alpha$*  HDFs. (a) The mRNA expression of *HIF-1 $\alpha$*  in control (CON313) and sh-*HIF-1 $\alpha$*  (73007, 73008, and 73009) HDFs determined using qRT-PCR ( $n=3$ ); (b–g) The protein expression of *HIF-1 $\alpha$* , LC3-II/LC3-I, Beclin-1, and p62 in control and sh-*HIF-1 $\alpha$*  HDFs determined by western blotting ( $n=3$ ); (h, i) Autophagy assessed as LC3 immunofluorescence intensity (magnification 400 $\times$ ;  $n=5$ ); (j–l) Apoptosis rates determined using flow cytometry ( $n=3$ ); (m, n) Cell proliferation determined using BrdU labeling (magnification 200 $\times$ ;  $n=3$ ); (o–q) Western blots of type III collagen and p53 ( $n=3$ ). \*  $P < 0.05$ , \*\*  $P < 0.01$ , \*\*\*  $P < 0.001$ , \*\*\*\*  $P < 0.0001$ . *HIF-1 $\alpha$* : hypoxia inducible factor-1 $\alpha$ ; HDF: human dermal fibroblast; LC3: light chain 3; Ctrl: control; mRNA: messenger RNA; qRT-PCR: quantitative real-time polymerase chain reaction; BrdU: 5-bromo-2'-deoxyuridine; DAPI: diamidine phenyl indole; sh-*HIF-1 $\alpha$* : short hairpin RNA (sh-RNA) was transfected by lentiviral vector to knock down *HIF-1 $\alpha$* .

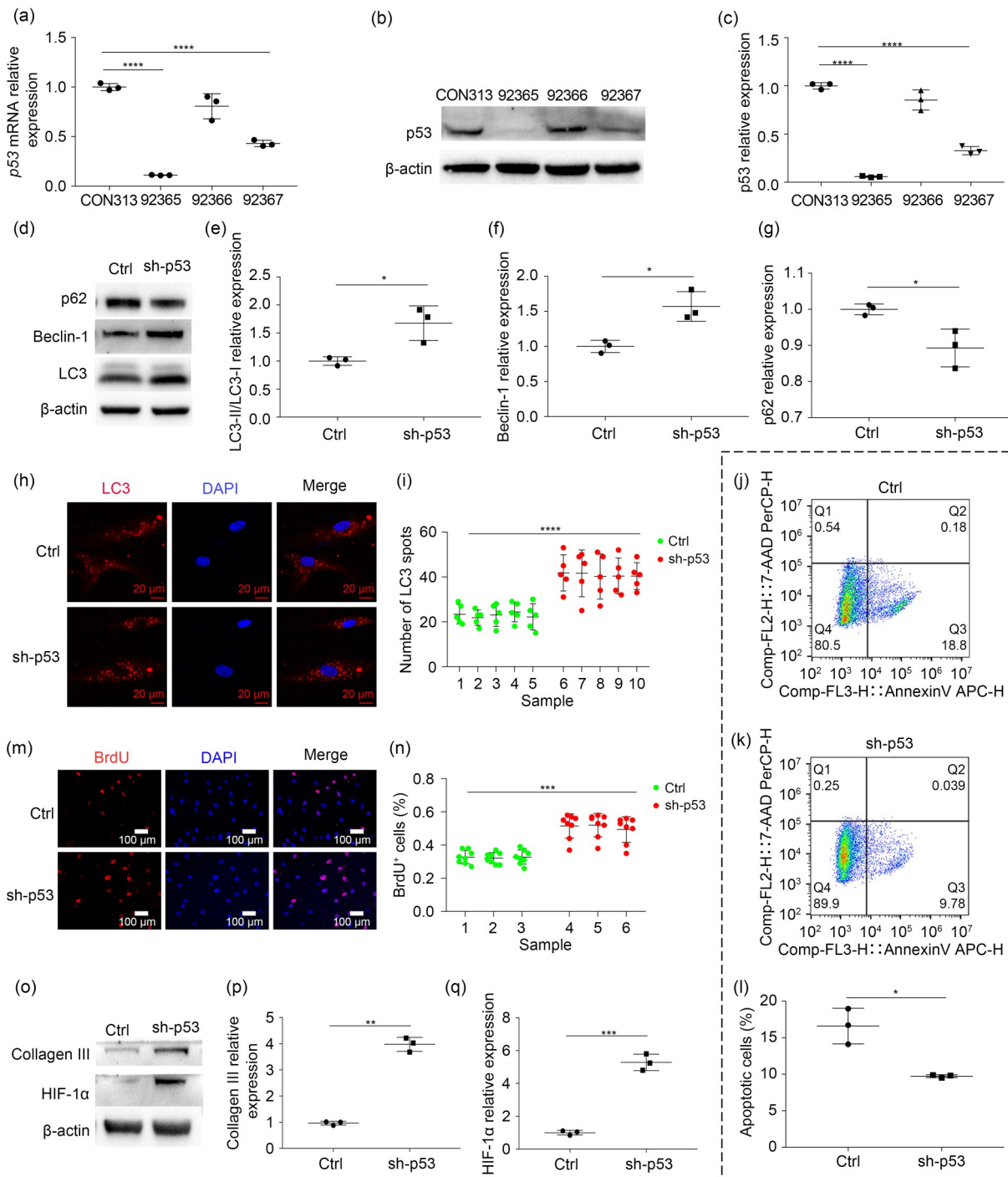


**Fig. 4** Autophagy, proliferation, and HIF-1 $\alpha$  expression levels are upregulated, whereas apoptosis and p53 expression are downregulated in sh-p53 HDFs under moderate hypoxia. (a) The mRNA expression of *p53* in control (CON313) and sh-p53 (92365, 92366, and 92367) HDFs determined using qRT-PCR ( $n=3$ ); (b–g) Western blots of p53, LC3-II/LC3-I, Beclin-1, and p62 protein expression in the control and sh-p53 HDFs ( $n=3$ ); (h, i) Autophagy assessed as LC3 immunofluorescence (magnification 400 $\times$ ;  $n=5$ ); (j–l) Apoptosis rates determined using flow cytometry ( $n=3$ ); (m, n) Cell proliferation determined by BrdU labelling (magnification 200 $\times$ ;  $n=3$ ); (o–q) Western blots of type III collagen and HIF-1 $\alpha$  ( $n=3$ ). \*  $P<0.05$ , \*\*  $P<0.01$ , \*\*\*  $P<0.0001$ , \*\*\*\*  $P<0.0001$ . HIF-1 $\alpha$ : hypoxia inducible factor-1 $\alpha$ ; HDF: human dermal fibroblast; LC3: light chain 3; Ctrl: control; mRNA: messenger RNA; qRT-PCR: quantitative real-time polymerase chain reaction; BrdU: 5-bromo-2'-deoxyuridine; DAPI: diamidine phenyl indole; sh-p53: short hairpin RNA (sh-RNA) was transfected by lentiviral vector to knock down *p53*.

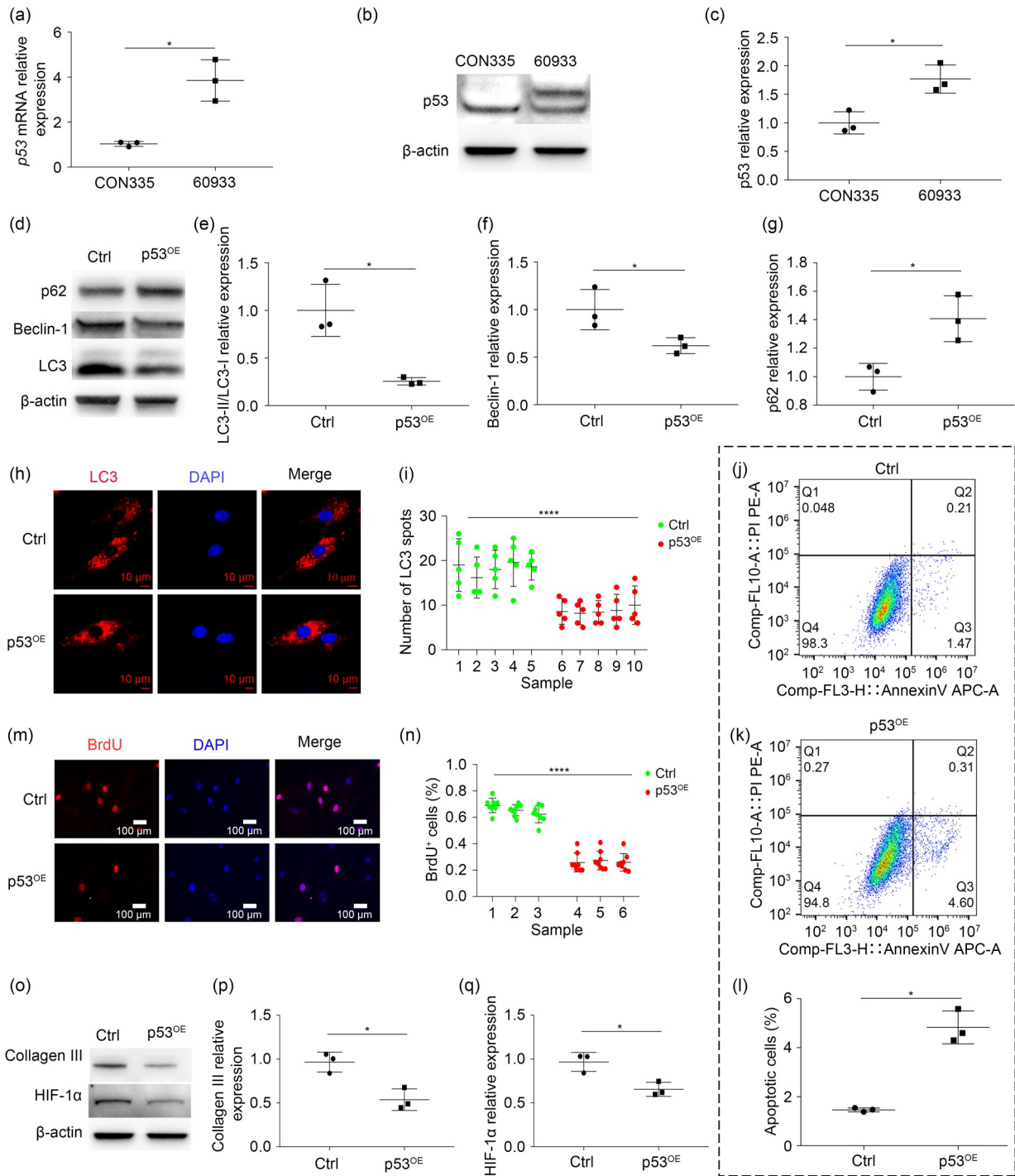


**Fig. 5** Autophagy, proliferation, and HIF-1 $\alpha$  expression are downregulated, while p53 expression and apoptosis are upregulated in p53<sup>OE</sup> HDFs under moderate hypoxia. (a) The mRNA expression of p53 in control (CON335) and p53<sup>OE</sup> (60933) determined in HDFs using qRT-PCR ( $n=3$ ); (b–g) Western blots of protein expression of p53, LC3-II/LC3-I, Beclin-1, and p62 ( $n=3$ ); (h, i) Autophagy assessed as LC3 immunofluorescence (magnification 400 $\times$ ;  $n=5$ ); (j–l) Apoptosis rates determined using flow cytometry (magnification 200 $\times$ ;  $n=3$ ); (m, n) Cell proliferation determined using BrdU labelling (magnification 200 $\times$ ;  $n=3$ ); (o–q) Western blots of type III collagen and HIF-1 $\alpha$  ( $n=3$ ). \*  $P<0.05$ , \*\*\*\*  $P<0.0001$ . HIF-1 $\alpha$ : hypoxia inducible factor-1 $\alpha$ ; HDF: human dermal fibroblast; LC3: light chain 3; Ctrl: control; mRNA: messenger RNA; qRT-PCR: quantitative real-time polymerase chain reaction; BrdU: 5-bromo-2'-deoxyuridine; DAPI: diamidine phenyl indole; p53<sup>OE</sup>: p53 overexpression.

(Figs. 5d–5g). Both the control and p53-overexpressing cells had LC3 fluorescent puncta, the number of which was lower in the latter group ( $P<0.0001$ ; Figs. 5h and 5i), indicating that autophagy was suppressed in p53<sup>OE</sup> HDFs. The flow cytometry revealed upregulated apoptosis in p53<sup>OE</sup> HDFs (Figs. 5j–5l). The relatively low ratios of BrdU-positive cells indicated reduced cell proliferation under p53 overexpression ( $P<0.0001$ ; Figs. 5m and 5n). The protein expression of type III collagen also decreased under p53 overexpression (Figs. 5o and 5p). These findings indicated that HIF-1 $\alpha$  expression, autophagy, and proliferation were downregulated, whereas p53 levels and apoptosis were enhanced under moderate hypoxia in p53<sup>OE</sup> HDFs. The data are shown in Table S2.

### 3.6 Competition between HIF-1 $\alpha$ and p53 for binding to transcription cofactor p300

In order to study the possible interaction pathways of HIF-1 $\alpha$  and p53, we immunoprecipitated total cell protein using a p300 antibody, and analyzed

HIF-1 $\alpha$  and p53 protein expression using western blotting to determine molecular interactions between them. Less HIF-1 $\alpha$  ( $P=0.0341$ ,  $P=0.0404$ ) and more p53 ( $P=0.0392$ ,  $P=0.0373$ ) bound to p300 in sh-HIF-1 $\alpha$  HDFs (Figs. 6a–6d) and p53<sup>OE</sup> HDFs (Figs. 6i–6l). The opposite trend was observed in sh-p53 HDFs ( $P=0.0036$ ,  $P=0.0012$ ; Figs. 6e–6h). These results indicated that HIF-1 $\alpha$  and p53 compete for binding to transcription cofactor p300.

## 4 Discussion

Dynamic hypoxia in HSs is closely associated with changes in fibroblast proliferation, as well as in collagen synthesis and secretion; however, the relevant mechanism remains obscure. In our study, immunohistochemical staining revealed increased HIF-1 $\alpha$  protein expression in the HS group, and electron microscopy indicated significantly upregulated autophagy in fibroblasts from HSs. We cultured

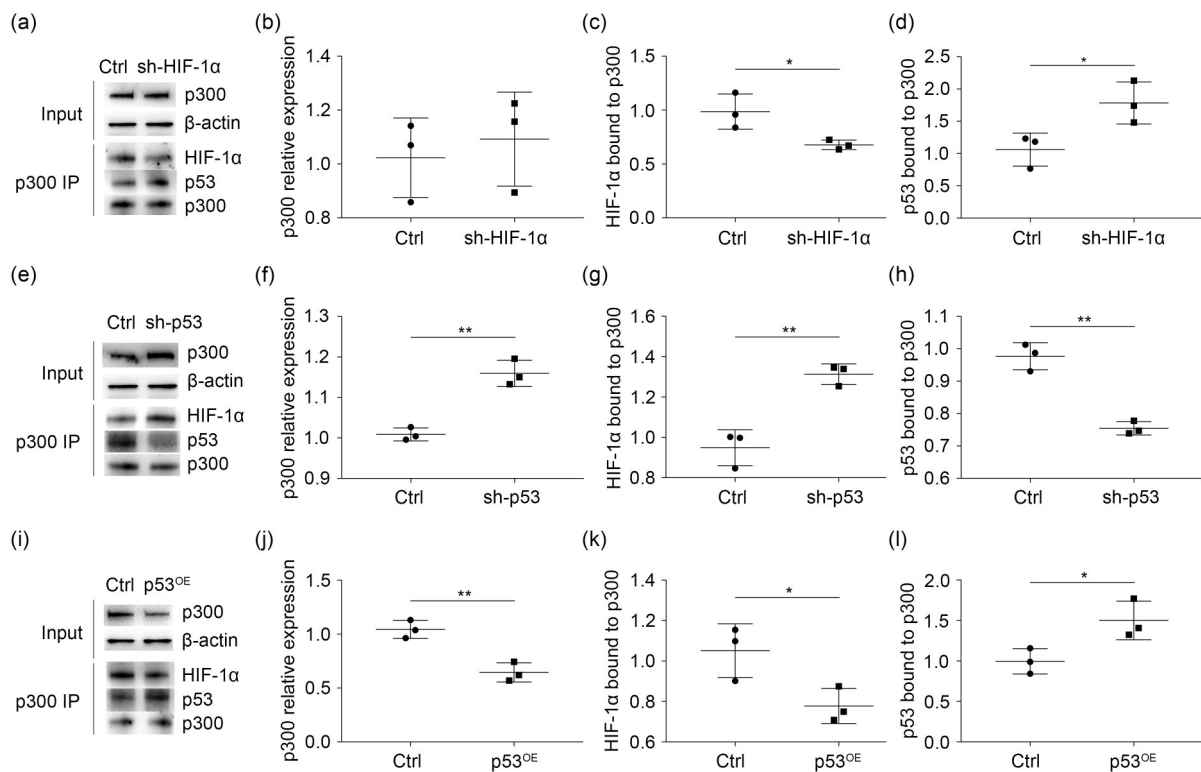


**Fig. 6** Functioning as transcription factors, HIF-1 $\alpha$  and p53 compete for binding to transcription cofactor p300. Immunoprecipitation shows amounts of HIF-1 $\alpha$  and p53 bound to p300 in the control and sh-HIF-1 $\alpha$  HDFs (a–d), sh-p53 HDFs (e–h), and p53<sup>OE</sup> HDFs (i–l) ( $n=3$ ). \* $P<0.05$ , \*\* $P<0.01$ . HIF-1 $\alpha$ : hypoxia inducible factor-1 $\alpha$ ; HDF: human dermal fibroblast; Ctrl: control; sh-HIF-1 $\alpha$ : short hairpin RNA (sh-RNA) was transfected by lentiviral vector to knock down *HIF-1 $\alpha$* ; sh-p53: sh-RNA was transfected by lentiviral vector to knock down *p53*; p53<sup>OE</sup>: *p53* overexpression; IP: immunoprecipitation.

HDFs under 5% O<sub>2</sub> to simulate moderate hypoxia in vitro, and found increased HIF-1 $\alpha$  expression, autophagy, cell proliferation, and type III collagen synthesis. Meanwhile, p53 expression and cell apoptosis were reduced, which confirmed the in vivo findings. However, in *HIF-1 $\alpha$*  gene knockdown, the autophagy-related proteins LC3-II/LC3-I and Beclin-1 were reduced along with cell proliferation and type III collagen levels, while p53 expression and apoptosis were elevated. HIF-1 $\alpha$  and p53 were regarded as the inducers of autophagy and apoptosis, and this change indicated a teeterboard-like conversion between HIF-1 $\alpha$  and p53.

Interestingly, when p53 expression was knocked down, HIF-1 $\alpha$  expression and autophagy were enhanced and apoptosis rates were lower, while cell proliferation increased in parallel with increased type III collagen synthesis. In contrast, when p53 was overexpressed, all of these indices showed the opposite effects and HIF-1 $\alpha$  expression was reduced. All of the evidence suggested that HIF-1 $\alpha$  and p53 expression exhibited a teeterboard-like conversion under hypoxic conditions, and the transition of autophagy and apoptosis in fibroblasts was dependent on the dominant expression of HIF-1 $\alpha$  or p53.

Previous findings have indicated that HIF-1 $\alpha$  and p53 might regulate each other (An et al., 1998; Schmid et al., 2004; Griggio et al., 2020; Lee et al., 2020). Furthermore, HIF-1 $\alpha$  interacts with p53 and could impair HIF-1 $\alpha$ -induced angiogenesis (Ravi et al., 2000), because both function as transcription factors that competitively bind the transcriptional cofactor p300 possessing acetyltransferase activity (Giordano and Avantaggiati, 1999) and play a key role in regulating hypoxia-related gene expression.

In our study, when *HIF-1 $\alpha$*  was knocked down, p300-bound HIF-1 $\alpha$  decreased, while p53 bound to p300 increased. The same phenomenon occurred under p53 overexpression, whereas p53 knockdown led to converse outcomes. These findings indicated that HIF-1 $\alpha$  and p53 not only regulate each other at the protein level, but also compete for transcriptional coactivator p300 binding. Co-transfection with p300 alleviates the p53-induced HIF-1 inhibition of transcriptional activity (Schmid et al., 2004). Thus, the transcriptional coactivator p300 may be a key modulator of HIF-1 $\alpha$  and p53 transcription factor activity. In addition, p53 knockdown and overexpression respectively increased and

reduced p300. The specific mechanism leading to this change in p300 warrants further investigation.

## 5 Conclusions

The present study identified a teeterboard-like conversion relationship between HIF-1 $\alpha$  and p53. The results also showed that changes in autophagy and apoptosis are dependent on the dominant expression of HIF-1 $\alpha$  and p53, which may play a significant role in the mechanism of scar hyperplasia and regression. Targeting HIF-1 $\alpha$ /p53 may reduce excessive fibroblast proliferation and consequent collagen deposition, and provide a theoretical basis for the development of novel HS therapeutics.

## Acknowledgments

This work was supported by the National Natural Science Foundation of China (No. 81671914).

## Author contributions

Min LI performed experiments, analyzed the data, and wrote the article. Yidan SU, Xiaoyuan GAO, and Jiarong YU performed experiments. Min LI, Xiqiao WANG, and Zhiyong WANG carried out the study design and article revision. All authors have read and approved the final manuscript, and therefore, have full access to all data in the study and take responsibility for the integrity and security of the data.

## Compliance with ethics guidelines

Min LI, Yidan SU, Xiaoyuan GAO, Jiarong YU, Zhiyong WANG, and Xiqiao WANG declare that they have no conflict of interest.

All procedures followed were in accordance with the ethical standards of the responsible committee on human experimentation (institutional and national) and with the Helsinki Declaration of 1975, as revised in 2008 (5). Informed consent was obtained from all patients for being included in the study.

## References

- An WG, Kanekal M, Simon MC, et al., 1998. Stabilization of wild-type p53 by hypoxia-inducible factor 1 $\alpha$ . *Nature*, 392(6674):405-408. <https://doi.org/10.1038/32925>
- Bjørkøy G, Lamark T, Brech A, et al., 2005. p62/SQSTM1 forms protein aggregates degraded by autophagy and has a protective effect on huntingtin-induced cell death. *J Cell Biol*, 171(4):603-614. <https://doi.org/10.1083/jcb.200507002>
- Chen YB, Niu ZH, Jiang WQ, et al., 2021. 3D-printed models improve surgical planning for correction of severe postburn

- ankle contracture with an external fixator. *J Zhejiang Univ-Sci B (Biomed & Biotechnol)*, 22(10):866-875.  
<https://doi.org/10.1631/jzus.B2000576>
- Deng MZ, Zhang WZ, Yuan LL, et al., 2020. HIF-1 $\alpha$  regulates hypoxia-induced autophagy via translocation of ANKRD37 in colon cancer. *Experim Cell Res*, 395(1):112175.  
<https://doi.org/10.1016/j.yexcr.2020.112175>
- Dong JY, Song F, Liu YK, et al., 2016. Effects of severe hypoxia and low concentration of serum protein on the function of human hypertrophic scar fibroblasts. *Chin J Burns*, 32(10):594-598 (in Chinese).  
<https://doi.org/10.3760/cma.j.issn.1009-2587.2016.10.005>
- Finnerty CC, Jeschke MG, Branski LK, et al., 2016. Hypertrophic scarring: the greatest unmet challenge after burn injury. *Lancet*, 388(10052):1427-1436.  
[https://doi.org/10.1016/S0140-6736\(16\)31406-4](https://doi.org/10.1016/S0140-6736(16)31406-4)
- Gauglitz GG, Korting HC, Pavicic T, et al., 2011. Hypertrophic scarring and keloids: pathomechanisms and current and emerging treatment strategies. *Mol Med*, 17(1-2):113-125.  
<https://doi.org/10.2119/molmed.2009.00153>
- Giordano A, Avantaggiati ML, 1999. p300 and CBP: partners for life and death. *J Cell Physiol*, 181(2):218-230.  
[https://doi.org/10.1002/\(SICI\)1097-4652\(199911\)181:2<218::AID-JCP>3.0.CO;2-5](https://doi.org/10.1002/(SICI)1097-4652(199911)181:2<218::AID-JCP>3.0.CO;2-5)
- Griggio V, Vitale C, Todaro M, et al., 2020. HIF-1 $\alpha$  is over-expressed in leukemic cells from TP53-disrupted patients and is a promising therapeutic target in chronic lymphocytic leukemia. *Haematologica*, 105(4):1042-1054.  
<https://doi.org/10.3324/haematol.2019.217430>
- Harris AL, 2002. Hypoxia—a key regulatory factor in tumour growth. *Nat Rev Cancer*, 2(1):38-47.  
<https://doi.org/10.1038/nrc704>
- He CC, Klionsky DJ, 2009. Regulation mechanisms and signaling pathways of autophagy. *Annu Rev Genet*, 43: 67-93.  
<https://doi.org/10.1146/annurev-genet-102808-114910>
- Ivan M, Kondo K, Yang HF, et al., 2001. HIF $\alpha$  targeted for VHL-mediated destruction by proline hydroxylation: implications for O<sub>2</sub> sensing. *Science*, 292(5516):464-468.  
<https://doi.org/10.1126/science.1059817>
- Jaakkola P, Mole DR, Tian YM, et al., 2001. Targeting of HIF- $\alpha$  to the von Hippel-Lindau ubiquitylation complex by O<sub>2</sub>-regulated prolyl hydroxylation. *Science*, 292(5516): 468-472.  
<https://doi.org/10.1126/science.1059796>
- Kabeya Y, Mizushima N, Ueno T, et al., 2000. LC3, a mammalian homologue of yeast Apg8p, is localized in autophagosome membranes after processing. *EMBO J*, 19(21): 5720-5728.  
<https://doi.org/10.1093/emboj/19.21.5720>
- Lee SH, Kang JH, Ha JS, et al., 2020. Transglutaminase 2-mediated p53 depletion promotes angiogenesis by increasing HIF-1 $\alpha$ -p300 binding in renal cell carcinoma. *Int J Mol Sci*, 21(14):5042.  
<https://doi.org/10.3390/ijms21145042>
- Levine B, Kroemer G, 2019. Biological functions of autophagy genes: a disease perspective. *Cell*, 176(1-2):11-42.  
<https://doi.org/10.1016/j.cell.2018.09.048>
- Liang YM, Zhou RP, Fu XJ, et al., 2021. HOXA5 counteracts the function of pathological scar-derived fibroblasts by partially activating p53 signaling. *Cell Death Dis*, 12:40.  
<https://doi.org/10.1038/s41419-020-03323-x>
- Lynam EC, Xie Y, Dawson R, et al., 2015. Severe hypoxia and malnutrition collectively contribute to scar fibroblast inhibition and cell apoptosis. *Wound Repair Regen*, 23(5): 664-671.  
<https://doi.org/10.1111/wrr.12343>
- Morishita H, Kaizuka T, Hama Y, et al., 2017. A new probe to measure autophagic flux in vitro and in vivo. *Autophagy*, 13(4):757-758.  
<https://doi.org/10.1080/15548627.2016.1278094>
- Nuñez-Hernandez DM, Felix-Portillo M, Peregrino-Uriarte AB, et al., 2018. Cell cycle regulation and apoptosis mediated by p53 in response to hypoxia in hepatopancreas of the white shrimp *Litopenaeus vannamei*. *Chemosphere*, 190:253-259.  
<https://doi.org/10.1016/j.chemosphere.2017.09.131>
- Pankiv S, Clausen TH, Lamark T, et al., 2007. p62/SQSTM1 binds directly to Atg8/LC3 to facilitate degradation of ubiquitinated protein aggregates by autophagy. *J Biol Chem*, 282(33):24131-24145.  
<https://doi.org/10.1074/jbc.M702824200>
- Qing C, Wang ZY, Song F, et al., 2016. Dynamic biological changes in fibroblasts during hypertrophic scar formation and regression. *Int Wound J*, 13(2):257-262.  
<https://doi.org/10.1111/iwj.12283>
- Ratcliffe PJ, O'Rourke JF, Maxwell PH, et al., 1998. Oxygen sensing, hypoxia-inducible factor-1 and the regulation of mammalian gene expression. *J Exp Biol*, 201(8):1153-1162.  
<https://doi.org/10.1242/jeb.201.8.1153>
- Ravi R, Mookerjee B, Bhujwala ZM, et al., 2000. Regulation of tumor angiogenesis by p53-induced degradation of hypoxia-inducible factor 1 $\alpha$ . *Genes Dev*, 14(1):34-44.  
<https://doi.org/10.1101/gad.14.1.34>
- Schmid T, Zhou J, Köhl R, et al., 2004. p300 relieves p53-evoked transcriptional repression of hypoxia-inducible factor-1 (HIF-1). *Biochem J*, 380(1):289-295.  
<https://doi.org/10.1042/BJ20031299>
- Schneider CA, Rasband WS, Eliceiri KW, 2012. NIH Image to ImageJ: 25 years of image analysis. *Nat Methods*, 9(7): 671-675.  
<https://doi.org/10.1038/nmeth.2089>
- Shieh SY, Ikeda M, Taya Y, et al., 1997. DNA damage-induced phosphorylation of p53 alleviates inhibition by MDM2. *Cell*, 91(3):325-334.  
[https://doi.org/10.1016/s0092-8674\(00\)80416-x](https://doi.org/10.1016/s0092-8674(00)80416-x)
- Sun YX, Yao X, Zhang QJ, et al., 2018. Beclin-1-dependent autophagy protects the heart during sepsis. *Circulation*, 138(20):2247-2262.  
<https://doi.org/10.1161/CIRCULATIONAHA.117.032821>
- van den Broek LJ, Limandjaja GC, Niessen FB, et al., 2014. Human hypertrophic and keloid scar models: principles, limitations and future challenges from a tissue engineering perspective. *Experi Dermatol*, 23(6):382-386.  
<https://doi.org/10.1111/exd.12419>

- Wang HK, Zhang DS, Jia SS, et al., 2018. Effect of sustained hypoxia on autophagy of genioglossus muscle-derived stem cells. *Med Sci Monit*, 24:2218-2224. <https://doi.org/10.12659/MSM.906195>
- Wu X, Li J, Yang XK, et al., 2018. miR-155 inhibits the formation of hypertrophic scar fibroblasts by targeting HIF-1 $\alpha$  via PI3K/AKT pathway. *J Mol Histol*, 49(4):377-387. <https://doi.org/10.1007/s10735-018-9778-z>
- Xia SX, Lv JX, Gao QQ, et al., 2015. Prenatal exposure to hypoxia induced Beclin 1 signaling-mediated renal autophagy and altered renal development in rat fetuses. *Reprod Sci*, 22(2):156-164. <https://doi.org/10.1177/1933719114536474>
- Zhang YP, Xiong Y, 2001. A p53 amino-terminal nuclear export signal inhibited by DNA damage-induced phosphorylation. *Science*, 292(5523):1910-1915. <https://doi.org/10.1126/science.1058637>
- Zheng JX, Song F, Lu SL, et al., 2014. Dynamic hypoxia in scar tissue during human hypertrophic scar progression. *Dermatol Surg*, 40(5):511-518. <https://doi.org/10.1111/dsu.12474>

**Supplementary information**

Tables S1 and S2